Available online at www.sciencedirect.com
ScienceDirect
Journal of the European Ceramic Society 27 (2007) 2503–2511
www.elsevier.com/locate/jeurceramsoc

Atomic force and scanning electron microscopy study of zirconia-coated silicon carbide fibers

N.I. Baklanova [a,*], B.N. Zaitsev [a], A.T. Titov [b]

[a] *Institute of Solid State Chemistry and Mechanochemistry, SB RAS, Kutateladze st. 18, Novosibirsk 630128, Russian Federation*
[b] *General Institute of Geology, Geophysics and Mineralogy, SB RAS, Novosibirsk 630090, Russian Federation*

Received 24 April 2006; received in revised form 18 August 2006; accepted 25 August 2006
Available online 27 September 2006

Abstract

The peculiarities of morphology of the initial Hi-Nicalon™ and Tyranno-SA™ fibers and also the zirconia-coated fibers before and after exposition to air at 1000 °C were studied using atomic force (AFM) and scanning electron microscopy (SEM). The quantitative AFM analysis allowed us to evaluate a number of roughness parameters of the initial and coated fibers. After application of coating, the roughness of Tyranno-SA™ fiber was increased approximately by a factor of 2 in comparison with that of the initial fiber for the same scanned squares, whereas the roughness parameters of Hi-Nicalon™ fiber retained its value after application of coating. Moreover, the difference in the roughness parameters for coated Tyranno-SA™ and Hi-Nicalon™ fibers is enhanced after exposition to air at 1000 °C. The grain sizes of coatings are also greatly distinct for both types of the coated and exposed to air fibers. It suggests that the microstructural properties of coatings studied are greatly dependent on the properties of fiber itself. The martensitic relief for the zirconia coating on Tyranno-SA™ fiber was directly observed by AFM.

The obtained results on roughness of coated ceramic fibers could be useful for the evaluation and optimization of the mechanical behavior of CMC's, e.g. SiC/ZrO_2/SiC_f.

Keywords: ZrO_2 coatings; SiC fibres; Electron microscopy

1. Introduction

The matrix/fiber interface plays a key role in the overall behavior of ceramic matrix composites (CMC's). For good mechanical composite properties, it is necessary that the fiber not only debond but also slide along the fiber/matrix interface.[1] The fiber/matrix sliding friction is proportional to the radial clamping stress on the fiber, which can be caused by residual normal stress arising from mismatch in coefficient of thermal expansion between fiber and matrix and from the roughness-induced radial stress.[2,3] The effect of roughness in the early stages of debond crack propagation can be pronounced and it is due to the initial unseating of the matching rough surfaces just behind the crack tip. This is why thorough investigation not only of the morphology of the coated fibers but also of topography and roughness must be fulfilled before their evaluation as constituents for CMC's.

Pyrocarbon and BN are commonly used as interphase materials, but they exhibit the environmental instability at operating temperatures. Among alternative interphases, the refractory oxide-based systems are considered as the most promising ones. Recently, the feasibility of ZrO_2 was demonstrated as a "weak" interfacial coating for SiC/SiC composites.[4,5] It was found that the CVD-ZrO_2 coating exhibited desired tensile failure behavior and extensive crack deflection within the interface region. Study of morphologic evolution of the CVD-ZrO_2 interfacial coating composed from mixture of tetragonal and monoclinic modifications revealed that a delamination within ZrO_2 layer occurred as result of the martensitic transformation of t-ZrO_2 nuclei to m-ZrO_2 on reaching a critical grain size and the development of significant compressive stresses due to volume dilation and shear associated with the martensitic $t \rightarrow m$ transformation. On this basis it was concluded that the $t \rightarrow m$ transformation is most likely the key mechanism responsible for the weak interface

* Corresponding author. Tel.: +7 383 3363839; fax: +7 383 3322847.
E-mail address: baklanova@solid.nsc.ru (N.I. Baklanova).

0955-2219/$ – see front matter © 2006 Elsevier Ltd. All rights reserved.
doi:10.1016/j.jeurceramsoc.2006.08.016

behavior. Sol–gel approach was proposed by Baklanova et al.[6] for production and retention of metastable tetragonal ZrO_2 interfacial coatings on Nicalon^{TM} fibers.

The aim of this work is to examine the surface roughness and morphology of two types of ceramic fibers Hi-Nicalon^{TM} and Tyranno-SA^{TM} with sol–gel derived *t*-ZrO_2 interfacial coatings using atomic force and scanning electron microscopy.

2. Experimental

2.1. Materials

Hi-Nicalon^{TM} (Nippon Carbon Co., Japan) and Tyranno-SA^{TM} (Ube Co., Japan) fiber tow were used as substrate materials. Prior to coating, Hi-Nicalon^{TM} fiber tow was immersed for 24 h in 50:50 acetone/ethanol mixture for removing a sizing agent, after that they were dried at ambient temperature. Then they were thermally treated in air at 450 °C. Tyranno-SA^{TM} fiber tow was immersed in hot water for desizing, dried at ambient temperature and heated in air at 500 °C.

The preparation of coated ceramic fibers was similar to that described in literature.[6] Sol–gel approach was used for preparation of multi-component rare earth oxide stabilized zirconia coatings on both types of ceramic fibers. At least two components were incorporated in conventional zirconia-yttria oxide system. Samples were named after the rare earth oxides content, i.e. 6Re-ZrO_2 means 6 mol% Re_2O_3 (where Re are rare earth elements) and 94 mol% ZrO_2. One and the same sol was used for fabrication of coatings on both types of ceramic fibers. The coating stage involved firstly the immersion of the ceramic fiber tow into sol, drying on air at ambient temperature and then slow heating firstly in air and then in argon flow at atmospheric pressure till 960 °C. To increase of thickness of interfacial coating, the dipping–annealing procedure was repeated several times. The Hi-Nicalon^{TM} and Tyranno-SA^{TM} fibers, as well as the zirconia-coated fibers before and after exposition to air at 1000 °C were investigated.

2.2. Specimen characterization

The morphology and composition of the initial and coated ceramic fibers before and after exposition to air at 1000 °C were examined by scanning electron microscope (SEM: LEO 1430VP). Elemental composition of coating was carried out using energy dispersive spectroscopy (EDS, Oxford).

The topography and surface roughness of fibers was examined by atomic force microscope (AFM) SolverP47Bio (NT-MDT, Russia) using contact and intermittent contact modes. Silicon cantilevers NSG11 (NT-MDT) were used. Filaments were attached to glass slide using double adhesive tape. Different areas of several filaments of each type fibers were selected randomly. A roughness and other statistical parameters of selected areas were obtained using tool "Statistics" from standard software of device. The AFM images were flattened before analysis using 2nd order surface subtraction. One can note that AFM technique dispenses with the necessity of any additional preparing of specimens for observation, whereas SEM technique needs in the deposition of a special Au conductive layer of ~20 nm thickness, and as a result any desired microstructural features of coatings can be obliterated.

3. Results and discussion

3.1. SEM/EDS analysis

SEM images of the initial and 6Re-doped ZrO_2 (one dipping–annealing cycle) coating on Tyranno-SA^{TM} fiber are represented in Fig. 1. One can see that the surface of the both

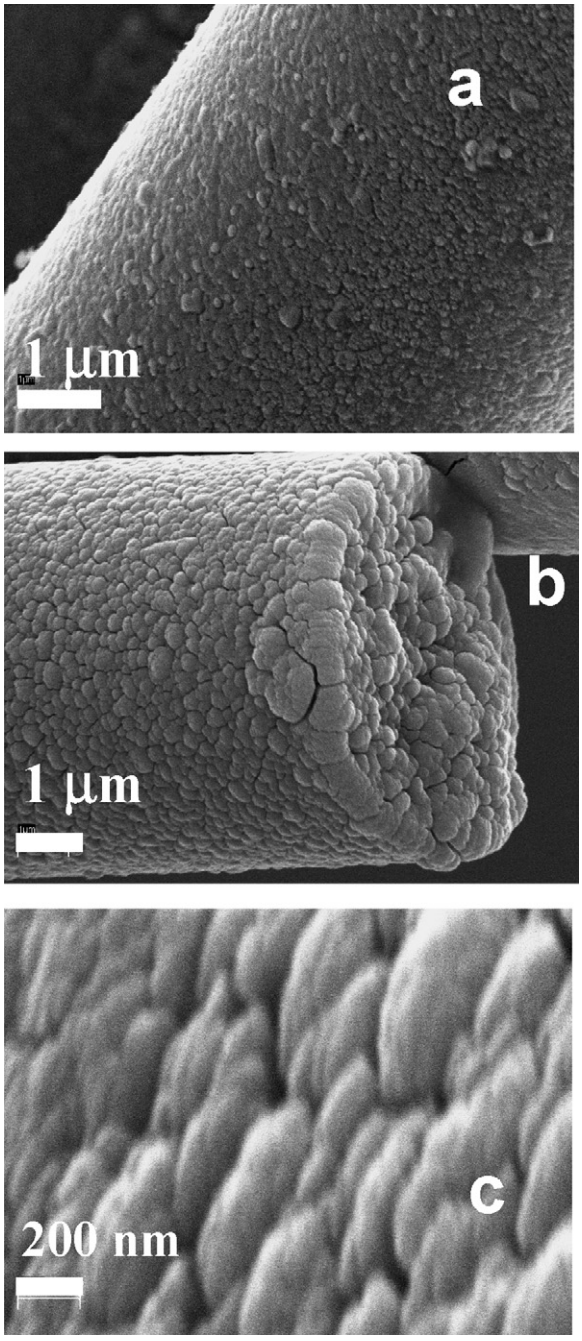

Fig. 1. (a–c) SEM images of the initial (a) and 6Re-ZrO_2-coated (one dipping–annealing cycle) Tyranno-SA^{TM} fiber.

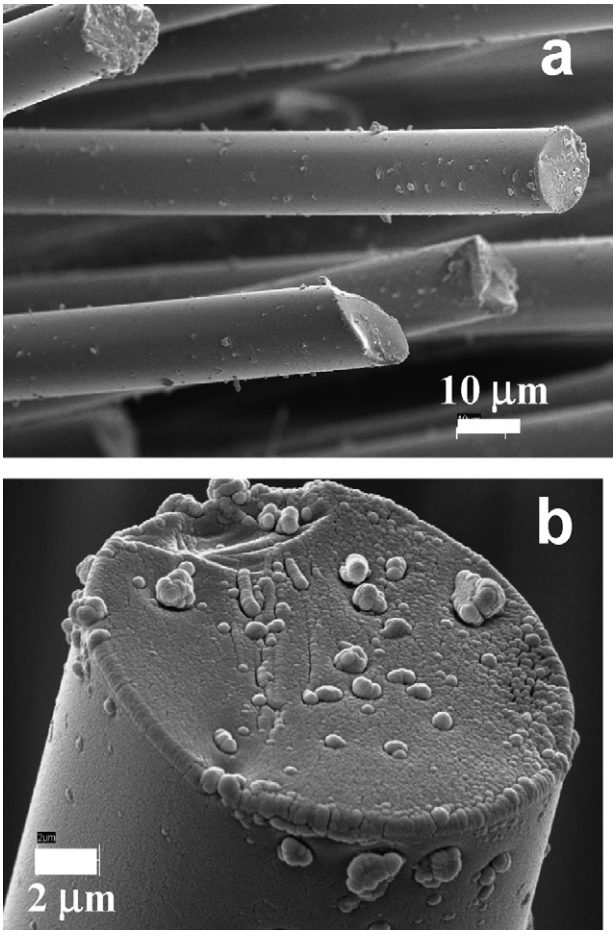

Fig. 2. (a and b) SEM images of the 6Re-ZrO_2-coated (one dipping–annealing cycle) Hi-Nicalon^{TM} fiber.

initial and coated fiber is rather rough and generally nodular in nature. Rather large nodules are present on the surface of separate coated monofilaments. This inhomogeneity appears to be as a consequence of pronounced inhomogeneity of the surface of the initial Tyranno type fiber that was mentioned earlier by Vanswijgenhoven.[7] From more close view of coated fiber one can see that the coating is composed of aggregates elongated in one direction (Fig. 1c), with size of separate aggregates in this direction being 200–400 nm. Fibers are not bridged by coating. No spalling of coating is observed. The thickness of coating after the first dipping–annealing cycle, determined by SEM, is about 400–500 nm. EDS showed that all of elements of coating are rather uniformly distributed through the surface of filament.

SEM images of the same type coating 6Re-doped ZrO_2 (one dipping–annealing cycle) on Hi-Nicalon^{TM} fiber are represented in Fig. 2a and b. A distinctive feature of this coating is smoothness and uniformity along length and diameter. Nevertheless, separate well-developed crystals can be seen on the surface. The thickness of coating is about 200–300 nm. In general, one can see that the surface of the both initial and coated Hi-Nicalon^{TM} fibers is smoother than that for Tyranno-SA^{TM}.

SEM images of the oxidized ceramic fibers show that the morphology of both coated fibers is somewhat changed after exposition to air at 1000 °C. Several peculiarities of oxidized coated Hi-Nicalon fibers can be detected (Fig. 3a–c). The surface of some filaments retains smoothness after exposition, whereas on the surface of the other filaments an appearance of a great number of well-developed columnar crystals was observed, with these crystals being preferentially lined up axially (Fig. 3a and b). The appearance of the bifurcation and zigzag pattern was observed on fracture surface of the oxidized Hi-Nicalon^{TM} fibers. Further, a delamination within the ZrO_2 interfacial coating is detected (Fig. 3d).

SEM images of the 6Re-ZrO_2 coated Tyranno-SA^{TM} fibers after exposition to air at 1000 °C are represented in Fig. 4a and b. One can see from SEM image of fracture surface that the thickness of coating is about 500 nm. No spalling of coating is observed and strong bonding between the fiber core and coating is retained after oxidation. The surface is rather rough and one can see that on some surface areas hills are disposed in a regular manner (Fig. 4b).

3.2. AFM analysis

3.2.1. AFM analysis of Tyranno-SA^{TM}

Some typical topographic views of the surfaces of the initial Tyranno-SA^{TM} fibers are represented in Fig. 5a–c. One can note that the surface is rather rough and hillocky. The disposition of the hills appears to be random. However, there are surface areas of the periodic disposition of hills (Fig. 5c), which are parallel to fiber axis. The most plausible reason for this regularity is related to extrusion process. Lateral sizes of particles are 100–200 nm, vertical sizes are 20–50 nm.

As one can see from Fig. 5, the surface is not homogeneous and rather large hills are neighboured by small ones. A quantitative analysis confirms this observation (Table 1). Here R_{max} gives the difference of the height values, R_{mean} the average value, R_a the roughness, R_q is a standard deviation

$$R_{max} = Z_{max} - Z_{min}.$$

$$R_{mean} = \frac{1}{N_x N_y} \sum_{i=1}^{N_x} \sum_{j=1}^{N_y} Zij$$

$$R_a = \frac{1}{N_x N_y} \sum_{i=1}^{N_x} \sum_{j=1}^{N_y} |z|$$

$$R_q = \sqrt{\frac{\sum_{i=1}^{N_x} \sum_{j=1}^{N_y} (z)^2}{N_x N_y}}$$

Although there is a considerable scatter of data, nevertheless, general trends are as follows. With increasing of scanned area the values of R_{max}, R_{mean}, R_a and R_q, are increased. Roughness of the initial Tyranno-SA^{TM} fiber is about 5 nm for scanned area of 1.7 μm^2.

As follows from Table 1, roughness is increased approximately by a factor of 2 after applying of the 6Re-ZrO_2 coating on Tyranno-SA^{TM} fiber (compare $R_a = 11.6$ nm for the coated and 5.1 nm for the initial fiber of the same scanned

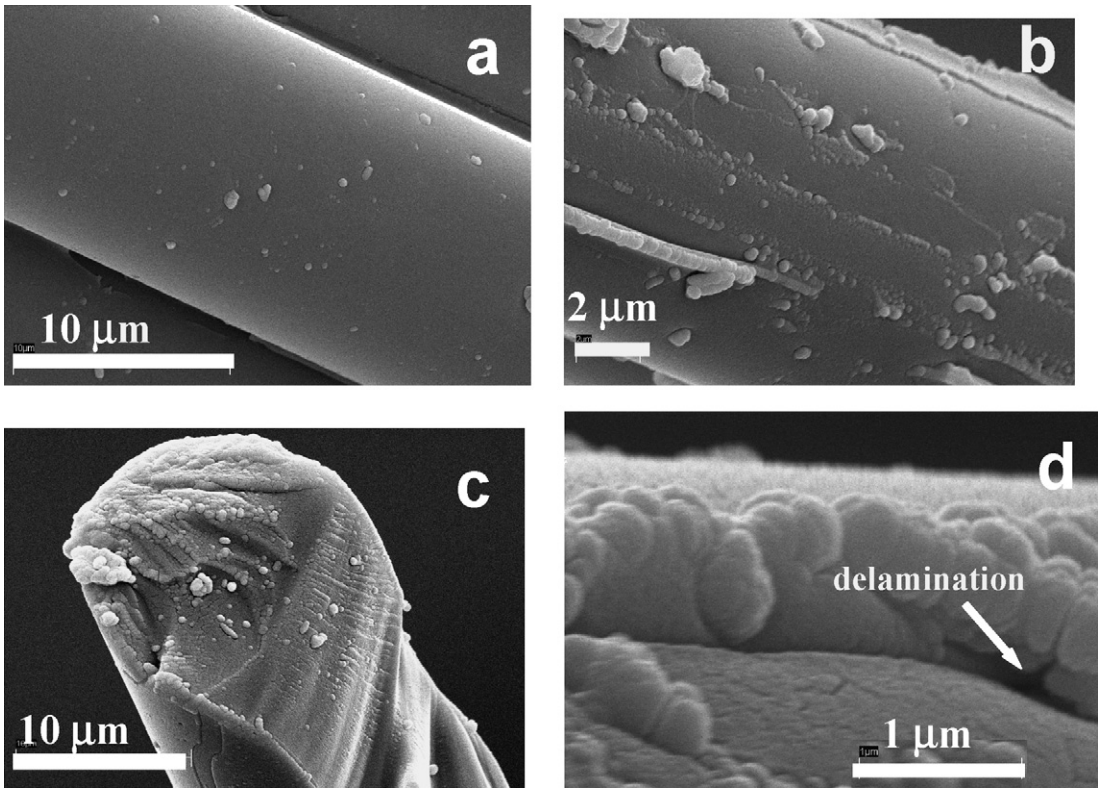

Fig. 3. (a–d) SEM images of the 6Re-ZrO_2-coated Hi-Nicalon^{TM} fibers after exposition to air at 1000 °C.

area 1.6–1.7 μm^2). Small precipitates are observed with well-developed habit planes. They group together into rows (Fig. 6b) and this structure is dominant feature for majority of filaments under study. Lateral sizes of particles are 100–200 nm, in some cases 500 nm.

After exposition to air at 1000 °C, the roughness of the coated fiber is also increased approximately by a factor of 2 (Table 1). One can see from Fig. 7a that the coating is composed of large grains. Some of particles are highly elongated in one direction and it could be proposed that they belong to monoclinic modification of ZrO_2. Besides, the separately disposed new formations of small size can be clearly seen from AFM image which was taken in the phase contrast mode.

More close view of relief allows us to detect an interesting feature (Fig. 7b, AFM deflection images), namely, rumpled structure. The presence of shear planes is clearly observed within some grains of the coating after exposition to air at elevated temperature. This picture is typical one for the $t \rightarrow m$ martensitic transformation in zirconia and one could be proposed that rumpled structure of surface results from this transformation. Invariant planes are indicated with arrows in Fig. 7b. This is direct observation of the $t \rightarrow m$ transformation within stabilized ZrO_2 interfacial coating. Earlier, the formation of self-accommodated martensite pairs induced by stress fields or ageing was observed by Chevalier and co-workers,[8,9] Chen et al. [10] and Tsubakino et al.[11] for zirconia monolithic ceramics using AFM.

Raman spectra of the 6Re-ZrO_2 coated Tyranno-SA^{TM} monofilaments before and after oxidation (not represented here) can serve as additional evidence in favor of $t \rightarrow m$ transformation within interfacial coating. Earlier, it was found using micro Raman spectroscopy that the 3YSZ coating on Nicalon^{TM} fiber exposed to air at elevated temperatures underwent the $t \rightarrow m$ transformation, with the extent of this transformation being different for various areas of the same filament and for various filaments.[12] According to Raman data of this work, the 6Re-ZrO_2 coating on Tyranno-SA^{TM} fiber is composed only

Table 1
The parameters used for characterization of the surface roughness of the initial and 6ReZrO_2-coated Tyranno-SA^{TM} fibers before and after exposition to air at 1000 °C

Fiber	Scanned area (μm^2)	R_{max} (nm)	R_{mean} (nm)	R_q (nm)	R_a (nm)
Tyranno-SA^{TM}	1.712	45.546	22.843	7.129	5.872
	7.088	84.561	30.382	9.330	7.397
Coated fiber before exposition	1.604	97.373	46.390	14.445	11.616
	8.567	139.943	48.396	18.230	14.571
Coated fiber after exposition	10.150	142.341	69.774	23.405	19.053
	8.590	210.618	132.090	35.048	27.846

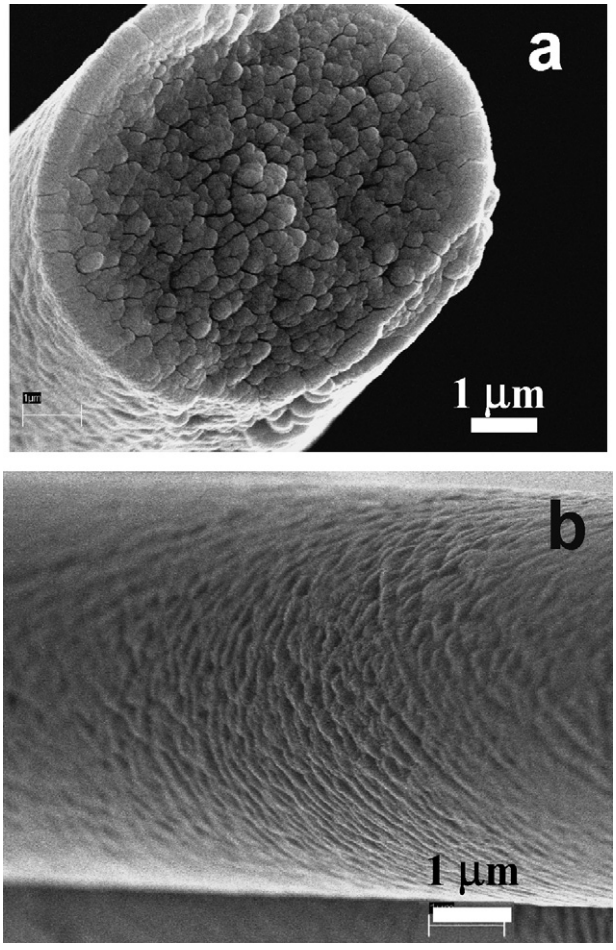

Fig. 4. (a and b) SEM images of the 6Re-ZrO_2-coated Tyranno-SA^{TM} fiber after exposition to air at 1000 °C.

of tetragonal modification before exposition. Additional Raman shifts were detected in micro Raman spectrum after exposition to air at 1000 °C and these peaks could be assigned to monoclinic ZrO_2 according to data.[13,14]

3.2.2. *AFM analysis of Hi-Nicalon*^{TM}

Topographic view of the surface of the desized Hi-Nicalon^{TM} fibers is represented in Fig. 8a. One can note that the surface is rather smooth. However, separate aggregates of large size can be seen and they can be originated from sizing agent. The surface layer is composed from particles of elongated shape. Results of quantitative analysis of relief of the desized Hi-Nicalon^{TM} fiber are represented in Table 2. The general trends are the same as for Tyranno-SA^{TM} fiber and the dependence of the roughness and other parameters on scanned areas is also observed.

The AFM image of the coated Hi-Nicalon^{TM} fiber is represented in Fig. 8b. One can see that the grains of coating have oblate ellipsoid forms with an aspect ratio of about 3. Lateral sizes are 120–150 nm. Grains have preferred orientation along axe of filament. And again, although there is a considerable scatter of data, nevertheless, one can note that the roughness of the Hi-Nicalon^{TM} fiber is 4–5 nm and changed not so drastically as in case for Tyranno-SA^{TM} fiber after application of the same type coating. The phase contrast mode enables us to detect the appearance of new phase in the coating on some Hi-Nicalon^{TM} filaments (Fig. 8c) but this is rare occurrence. One can propose that the formation of new phase appears to be initiated preferentially in places of junction of planes and then propagates inside of grains. Additional studies must be fulfilled to clarify a nature of these transformations.

The roughness parameters for the 6Re-ZrO_2 coated Hi-Nicalon^{TM} fiber after exposition to air at 1000 °C are approximately of the same order of magnitude as for fibers before exposition (Table 2), whereas the habit is changed, namely, columnar ZrO_2 crystals are clearly observed using AFM (Fig. 8d). It should be noted that the features of transformed zones were also detected on the surface of coated Hi-Nicalon^{TM} fibers and rumpled relief as one of the most important characteristics of martensitic transformation is clearly seen in Fig. 9. This figure shows that some *m* laths formed in *t* grains are parallel to each other. Owing to a high vertical resolution of AFM it is possible to make direct observation of martensitic relief and to measure its sizes.

4. Discussion

Several results concerning the peculiarities of relief of the desized, 6Re-ZrO_2 coated Hi-Nicalon^{TM} and Tyranno-SA ^{TM} fibers before and after exposition to air must be discussed in more details. At first, both SEM and AFM data are in agreement with each other for both types of ceramic fibers. Indeed, the SEM and AFM analysis data show that native relief of Tyranno-SA^{TM} fiber is very rough and some periodicity in disposition of grains as a result of fiber processing can be observed. The analogous regularities, namely, the appearance of periodical disposition of asperities on the surface of native filaments as a consequence of

Table 2
The parameters used for characterization of the surface roughness of the initial and 6ReZrO_2-coated Hi-Nicalon^{TM} fibers before and after exposition to air at 1000 °C

Fiber	Scanned area (μm^2)	R_{max} (nm)	R_{mean} (nm)	R_q (nm)	R_a (nm)
Hi-Nicalon^{TM}	3.402	92.993	50.868	7.745	5.574
	0.923	74.973	28.591	6.934	5.119
Coated fiber before exposition	2.799	92.412	86.608	13.408	9.250
	0.9051	36.701	17.598	5.019	4.021
Coated fiber after exposition	6.108	60.011	82.882	6.224	4.929
	2.126	60.424	16.872	4.100	3.197

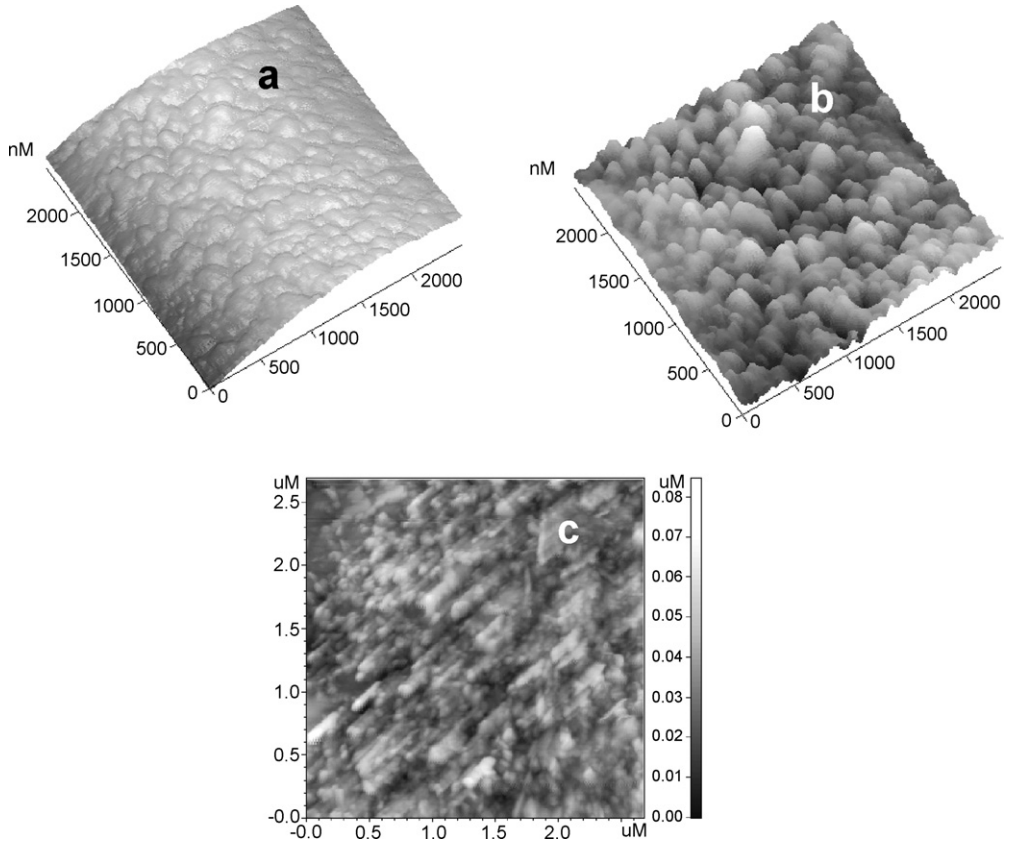

Fig. 5. (a–c) AFM images of the initial Tyranno-SA^{TM} fiber: (a) 3D image; (b) 3D image after subtraction of 2nd order surface; (c) 2D image of area of disposition of hills. Color bar shows distribution of heights.

extrusion process, were also observed for Hi-Nicalon^{TM} fibers. Thus, microstructure of both types of the initial ceramic fibers is characterized by ordering in disposition of grains of upper layers.

Relief of the applied 6Re-ZrO_2 coating is strongly affected by native relief of fiber itself. The morphology of zirconia crystals (oblate ellipsoids) of coating on Hi-Nicalon^{TM} filaments is distinct from that (columnar) for coating on Tyranno-SA^{TM} filaments. The observed differences in morphology could result from the differences in habit plane orientation towards substrate at the early stages of precipitation of ZrO_2 crystals.[15,16] Another distinct feature of the 6Re-ZrO_2 coating on Hi-Nicalon^{TM} fiber is the smoother relief and the lower values of roughness parameters in comparison with those for the same type of coating

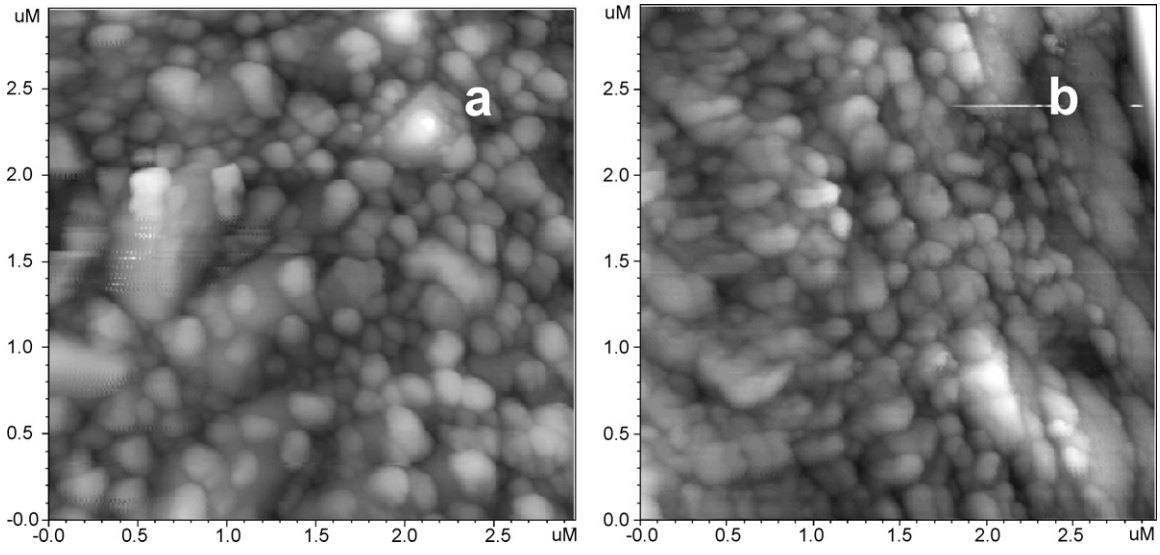

Fig. 6. (a and b) AFM images of the 6Re-ZrO_2-coated (one dipping–annealing cycle) Tyranno-SA ^{TM} fiber.

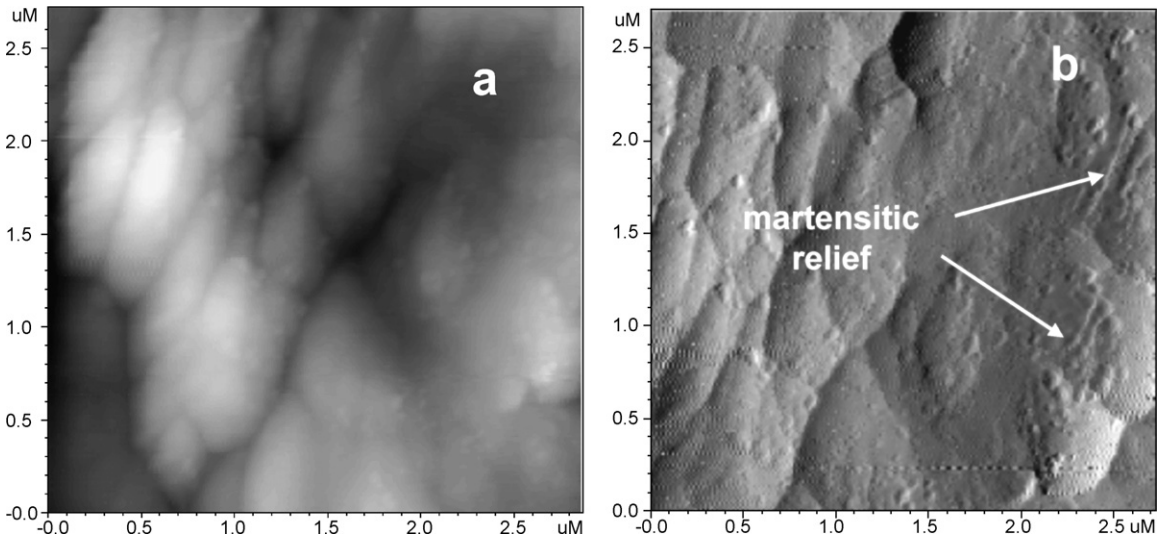

Fig. 7. (a and b) AFM images of the 6Re-ZrO_2-coated (one dipping–annealing cycle) Tyranno-SA^{TM} fiber exposed to air at 1000 °C: (a) the height mode; (b) phase mode.

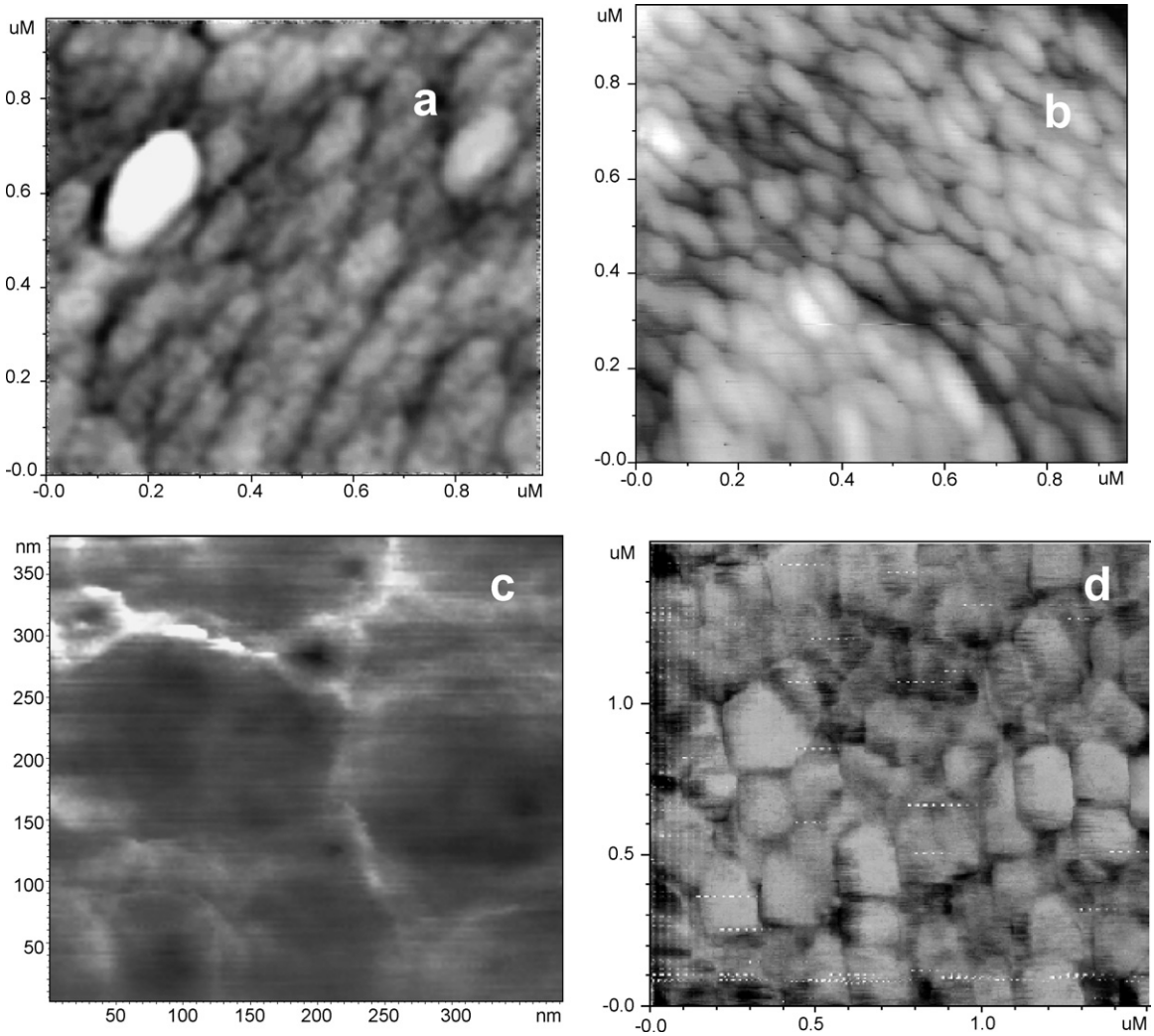

Fig. 8. (a–d) AFM image of Hi-Nicalon^{TM} fiber: (a) the initial fiber; (b) 6Re-ZrO_2-coated (the height mode); (c) 6Re-ZrO_2-coated (the phase contrast mode); (d) after exposition to air at 1000 °C (the lateral mode).

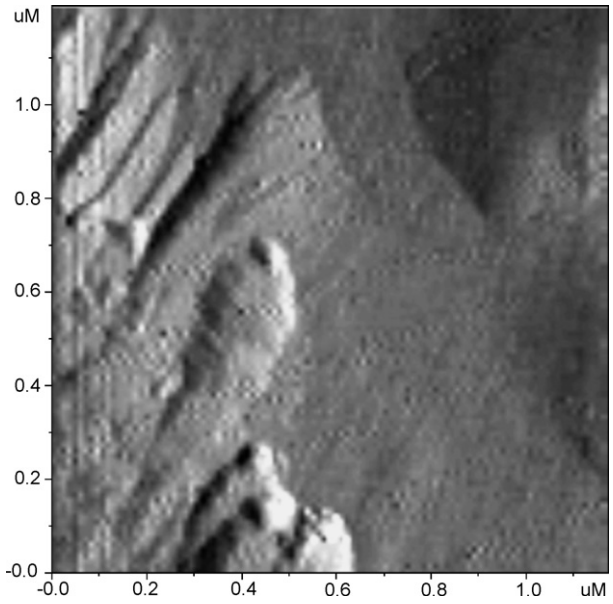

Fig. 9. AFM image of martensite relief of coated Hi-Nicalon fiber after exposition to air at 1000 °C.

on Tyranno-SA^{TM} fiber. This is of critical importance during fiber sliding because of high amplitude R_{max} magnitudes may serve as an obstacle to sliding. According to model by Kerans et al.,[2] the roughness-induced radial stress on the fiber from matrix in CMC's is proportional to $(-A/r)$, where A is characteristic roughness amplitude and r is radius of fiber. One could be expected that the roughness-induced radial stress on the coated Tyranno-SA^{TM} fiber from ceramic matrix would be higher in comparison with that on the coated Hi-Nicalon^{TM} fiber because of the higher roughness and the less radius of filament. One can note that there are various scenarios of matrix crack propagation following by debonding on the matrix/coating, coating/fiber interfaces or within interfacial coating. Therefore, the roughness parameters of the initial, coated and exposed to air fibers can be useful for evaluation of overall mechanical properties of composites in dependence of scenario.

Another question to be discussed is the morphological features of both types of coated fibers after exposition to air at high temperature. As was mentioned above, the presence of shear planes is clearly observed within some grains of the 6Re-ZrO_2 coating on both Tyranno-SA^{TM} and Hi-Nicalon^{TM} fibers after exposition to air at 1000 °C. It is well documented that the appearance of self-accommodating pairs of planes is a feature of the $t \rightarrow m$ martensitic transformation in zirconia. One of the reasons for observable $t \rightarrow m$ transformation can be an environmental degradation of zirconia coatings stabilized by rare earth oxides. Despite of numerous works devoted to the environmental degradation phenomenon of zirconia ceramics [see, e.g. review[17]], the nature of this process has not been fully understood. According to these studies, the mechanism of degradation is based on the formation of Zr–OH and Y–OH bonds at the surface of grains after adsorption water with following migration of the OH^- ions into interior of grains and occupation vacancy sites. This in turn generates stressed regions that can act as nucleating agents for the $t \rightarrow m$ transformation. The fact that no any transformation was detected for the 6Re-ZrO_2 coating on Tyranno-SA^{TM} and Hi-Nicalon^{TM} fibers during processing under vacuum conditions is evidence in favor of an environmental degradation as dominant factor for triggering the tetragonal–monoclinic phase transformation. On the other hand, the intrinsic phase stability of a tetragonal stabilized zirconia grains decreases as grain size increases due to the increase in microstructural defects, such as dislocations and residual stresses.[18,19] Although the environmental degradation itself is depend on grain size in complicated manner, one can propose that in this case both factors, namely, the interaction with water vapor and the increase in grain sizes, facilitate the $t \rightarrow m$ transformation.

As was mentioned above, the different areas of Re-ZrO_2 coating on ceramic fibers undergo the $t \rightarrow m$ phase transformation to different extent (Fig. 7a and b). This fact is in good agreement with micro Raman data obtained earlier by Baklanova et al.[12] for YSZ coatings on Nicalon^{TM} fibers. The observable difference could be caused by micro heterogeneity of the coating, including the grains sizes, reactivity towards water vapor, presence of defects, the stress level within grains, inhomogeneity of elemental composition of coating. The micro heterogeneity of coatings was also confirmed by AFM and SEM studies in this work.

5. Conclusion

The peculiarities of morphology of the initial Hi-Nicalon^{TM} and Tyranno-SA^{TM} fibers and also the 6Re-ZrO_2-coated fibers before and after exposition to air at 1000 °C were studied using atomic force and scanning electron microscopy. The quantitative AFM analysis allowed us to evaluate a number of roughness parameters of the initial and coated fibers.

In this work, both Tyranno-SA^{TM} and Hi-Nicalon^{TM} fibers were coated under the same conditions using the same stabilized-ZrO_2 sol. Due to this fact, some characteristics of coatings on both types of fibers are similar, for example, uniformity along length and diameter. The presence of large crystals on surface of both coated fibers is a rare occurrence. However, despite of the same sol for coating process, some characteristics of coatings differ from each other. As was shown using the quantitative AFM analysis, after application of coating the roughness of Tyranno-SA^{TM} fiber was increased approximately by a factor of 2 in comparison with that of the initial fiber, whereas the roughness parameters of Hi-Nicalon^{TM} fiber retained its value after application of coating. Moreover, the difference in the roughness parameters for coated Tyranno-SA^{TM} and Hi-Nicalon^{TM} fibers is enhanced after exposition to air at 1000 °C. The grain sizes of coatings are also greatly distinct for both types of the coated and exposed to air fibers. It suggests that the microstructural properties of coatings studied are greatly depend on the properties of fiber itself.

The $t \rightarrow m$ martensitic transformation in the 6Re-ZrO_2 interfacial coating on both types ceramic fibers was directly observed using AFM. An environmental degradation and the increase in grain sizes can be considered as factors to facilitate the $t \rightarrow m$ transformation.

The obtained results on roughness of coated ceramic fibers can be significant in its consequences for evaluation of the mechanical behavior of CMC's, e.g. $SiC/ZrO_2/SiC_f$. Indeed, in CMC's several well-identified mechanisms, namely, matrix microcracking, fiber/matrix debonding and fiber pullout contribute to increase the work of fracture and resistance to crack propagation and to avoid of catastrophic failure. Among above listed mechanisms, debonding and sliding of fibers relative to the matrix are strongly dependent on properties of interfacial coatings, especially on the fiber surface roughness parameters. Therefore, the obtained results could be used as design parameters for optimization of CMC's composites in future.

Acknowledgements

The authors would like to thank Prof. A. Kohyama (Kyoto Technological University) for supplying Tyranno-SA^{TM} fibers. The authors are grateful to Dr. Sci. B.A. Kolesov (Institute of Inorganic Chemistry SB RAS, Novosibirsk) for micro Raman studies.

References

1. Kerans, R. J., Hay, R. S., Parthasarathy, T. A. and Cinibulk, M. K., Interface design for oxidation-resistant ceramic composites. *J. Am. Ceram. Soc.*, 2002, **85**(11), 2599–2632.
2. Parthasarathy, T. A., Barlage, D. R., Jero, P. D. and Kerans, R. J., Effect of interfacial roughness parameters on the fiber pushout behavior of a model composite. *J. Am. Ceram. Soc.*, 1994, **77**(12), 3232–3236.
3. Jero, P. D., Kerans, R. J. and Parthasarathy, T. A., Effect of interfacial roughness on the frictional stress measured using pushout tests. *J. Am. Ceram. Soc.*, 1991, **74**(11), 2793–2801.
4. Li, H., Lee, J., Libera, M. R., Lee, W. Y., Kebbede, A., Lance, M. J. *et al.*, Morphological evolution and weak interface development within chemical-vapor-deposited zirconia coating deposited on Hi-Nicalon^{TM} fiber. *J. Am. Ceram. Soc.*, 2002, **85**(6), 1561–1568.
5. Li, H., Morsher, G. N., Lee, J. and Lee, W. Y., Tensile and stress-rupture behavior of SiC/SiC minicomposite containing chemically vapor deposited zirconia interphase. *J. Am. Ceram. Soc.*, 2004, **87**(9), 1726–1733.
6. Baklanova, N. I., Titov, A. T., Boronin, A. I. and Kosheev, S. V., The yttria-stabilized zirconia interfacial coating on Nicalon^{TM} fiber. *J. Eur. Ceram. Soc.*, 2006, **26**(9), 1725–1736.
7. Vanswijgenhoven, E., Lambrinou, K., Wevers, M. and Van Der Biest, O., Comparative study of the surface roughness of nicalon and tyranno silicon carbide fibres. *Composites Part A*, 1998, **29A**(11), 1417–1423.
8. Deville, S., Attaoui, H. E. and Chevalier, J., Atomic force microscopy of transformation toughening in ceria-stabilized zirconia. *J. Eur. Ceram. Soc.*, 2005, **25**(13), 3089–3096.
9. Deville, S. and Chevalier, J., Martensitic relief observation by atomic force microscopy in yttria stabilized zirconia. *J. Am. Ceram. Soc.*, 2003, **86**(12), 2225–2227.
10. Chen, X. Y., Zheng, X. H., Fang, H. S., Shi, H. Z., Wang, X. F. and Chen, H. M., The study of martensitic transformation and nanoscale surface relief in zirconia. *J. Mater. Sci. Lett.*, 2002, **21**(5), 415–418.
11. Tsubakino, H., Kuroda, Y. and Niibe, M., Surface relief associated with isothermal martensite in zirconia-3 mol%-yttria ceramics observed by atomic force microscopy. *J. Am. Ceram. Soc.*, 1999, **82**(10), 2921–2923.
12. Baklanova, N. I., Kolesov, B. A. and Zima, T. M., Raman study of yttria stabilized zirconia interfacial coatings on Nicalon^{TM} fiber. *J. Eur. Ceram. Soc.*, 2007, **27**, 165–171.
13. Lopez, E. F., Escribano, V. S., Panizza, M., Carnasciali, M. M. and Busca, G., Vibrational and electronic spectroscopic properties of zirconia powders. *J. Mater. Chem.*, 2001, **11**(7), 1891–1897.
14. Phillippi, C. M. and Mazdiyasni, K. S., Infrared and Raman spectra of zirconia polymorphs. *J. Am. Ceram. Soc.*, 1971, **54**(5), 254–258.
15. Babad-Zachryapin, A. A. and Kuznetsov, G. D., *Textured High-Temperature Coatings*. Atomizdat, Moscow, 1980, pp. 9–16.
16. Lanteri, V., Mitchell, T. E. and Heuer, A. H., Morphology of tetragonal precipitates in partially stabilized ZrO_2. *J. Am. Ceram. Soc.*, 1986, **69**(7), 564–569.
17. Lawson, S., Environmental degradation of zirconia ceramics. *J. Eur. Ceram. Soc.*, 1995, **15**(6), 485–502.
18. Guo, X., On the degradation of zirconia ceramics during low-temperature annealing in water or water vapor. *J. Phys. Chem. Solids*, 1999, **60**(4), 539–546.
19. Li, J.-F. and Watanabe, R., Phase transformation in Y_2O_3-partially-stabilized ZrO_2 polycrystals of various grain sizes during low-temperature aging in water. *J. Am. Ceram. Soc.*, 1998, **81**(10), 2687–2691.